Journal of Hydrology 664 (2026) 134406

Contents lists available at ScienceDirect

Journal of Hydrology

journal homepage: www.elsevier.com/locate/jhydrol

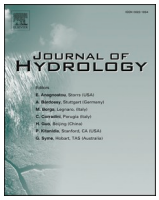

Variability of urban riverine nutrients under coupled human-hydrological-biogeochemical framework

Ying Zhang, Jianping Gan *

Department of Ocean Science, Department of Mathematics and Center for Ocean Research in Hong Kong and Macau, Hong Kong University of Science and Technology, Hong Kong, China

ARTICLE INFO

This manuscript was handled by Huaming Guo, Editor-in-Chief, with the assistance of Mengqi Jia, Associate Editor

Keywords:
Anthropogenic source
Instream process
River delta
Water quality

ABSTRACT

Nutrient fluxes exhibit complex dynamics under combined influences of land surface processes and human activities. In this study, we comprehensively investigate the long-term variability of riverine nutrient fluxes and uncover the underlying controlling mechanisms in a typical urban agglomeration by integrating observations with the Export Coefficient Model and the Soil and Water Assessment Tool within a coupled human-hydrological-biogeochemical framework. Our results show that the non-point sources (NPS) pollution is controlled by coupled transport processes and nutrient sources. High surface flows in urban and agricultural areas, actively combined with their respective nitrogen deposition and intensive fertilizer use, form active NPS zones. In forested regions, elevated nitrogen levels result from soil nitrate leaching in the lateral layer, where lateral flow is not a limiting factor. The elevated riverine nitrogen flux from NPS, relative to phosphorus, results from the combined effects of abundant nutrient inputs and a disproportionately higher export rate of nitrogen. In contrast, point sources are primarily driven by domestic wastewater, which establishes a persistent core-periphery pollution structure in urban agglomerations, with intensity decreasing from domestic-heavy and hybrid-sourced areas at the core to agro-centric regions at the periphery. However, this structure weakens as domestic sources decline significantly while non-domestic sources remain dynamically balanced. Regarding instream processes, nutrient transformation and removal in channels are positively influenced by organic nutrient ratios and transport distance, whereas upstream influx has a relatively minor impact. These findings provide valuable insights into riverine nutrient pollution from various sources across diverse landscapes in urban agglomerations worldwide.

1. Introduction

Riverine nutrient flux is vital for the health of aquatic ecosystems and ensuring human sustainability (Battin et al., 2023). It has changed globally due to agricultural expansion and urbanization, which directly or indirectly alter nutrient inputs into rivers (McDowell et al., 2025). Additionally, land surface processes significantly influence the transport and transformation of nutrients from landscapes into river networks (Hale et al., 2015). The interplay of human, hydrological, and biogeochemical processes complicates the identification of the mechanisms controlling nutrient flux, thereby hindering effective water quality management (Tang et al., 2022).

Nutrient flux displays dynamic spatiotemporal patterns during urban agglomeration development (Deng et al., 2023). The Environmental Kuznets Curve (EKC) framework hypothesizes an inverted U-shaped relationship between economic growth and environmental pollution. In the early stages of economic development, water pollution increases as industries and populations expand, but it declines after a critical turning point, primarily due to stricter regulations and improvements in wastewater treatment (Santis et al., 2024). This inverted U-shaped temporal pattern has been widely observed in regions such as China, North America, and Europe (Hildebrandt et al., 2024). Spatially, nutrient intensity generally decreases from central cities, dominated by domestic activities, to peripheral regions characterized by agricultural activities (Cheshmehzangi and Tang, 2022).

While these patterns are well-documented, variations of nutrient sources in the associated cities may deviate from the typical EKC pattern. For instance, nutrients from rural domestic sources may continue to decline due to urbanization and improved sewage systems, while nutrient fluxes from livestock and aquaculture may fluctuate in response to macroeconomic policies and shifts in dietary preferences (Sun et al., 2023). Central cities often reduce nutrient flux by

* Corresponding author.
E-mail address: magan@ust.hk (J. Gan).

https://doi.org/10.1016/j.jhydrol.2025.134406
Received 15 June 2025; Received in revised form 11 September 2025; Accepted 7 October 2025
Available online 10 October 2025

transitioning to green industries after the EKC turning point; however, peripheral regions may inherit high-pollution industries relocated from urban cores, leading to opposing trends within urban agglomerations. These deviations highlight the pressing need for long-term, city-level investigations into nutrient flux patterns across diverse sources.

Non-point sources (NPS) of nutrients are the dominant contributors to global riverine nutrient fluxes, regulated by complex biogeochemical cycles within climate-vegetation-soil systems (Ongley et al., 2010). Among these sources, agricultural fertilizers play a leading role, especially in regions like China, where excessive fertilizer use accounts for 30 % of global consumption, despite low use efficiency (Ju et al., 2016). In contrast, natural nutrient sources have received comparatively less attention (Chen et al., 2022). For instance, the decomposition of plant debris and crop residues releases various nutrients into the soil (Wang et al., 2024). Atmospheric deposition also supplies considerable amounts of nitrogen, which enhances soil fertility and subsequently enters aquatic ecosystems. Beyond these soil nutrient cycling, nutrient species also change within instream environments, involving various biotic and abiotic processes in the water column and riverbed (Li et al., 2024). Therefore, a comprehensive understanding of riverine nutrient fluxes necessitates clear insights into the linkages between nutrient inputs and losses driven by various biogeochemical processes.

Terrestrial hydrology significantly influences the transport of NPS nutrients across land surfaces. Runoff is a primary driver of interannual and seasonal variations in riverine nutrient fluxes, with substantial nutrient transport during rainy seasons and in wet years. The high kinetic energy of surface flow actively mobilizes nutrients from the topsoil and contributes to soil splash (Zhang et al., 2024). In contrast, the transport of NPS nutrients in subsoils, facilitated by subsurface flow, remains poorly understood (Nakayama et al., 2025). Nutrients in subsoils originate from topsoil leaching and the decomposition of detritus. Furthermore, biological uptake and microbial processes influence soil nutrient availability, resulting in higher nutrient concentrations in soil solutions compared to stream water (Mihiranga et al., 2022). These nutrient pathways within the soil profile highlight the necessity of identifying the roles of different flow components.

Land use plays a critical role in regulating the biogeochemical processes associated with nutrient flux on land surfaces. Agricultural lands receive intensive fertilizers, whereas forested regions experience elevated nitrogen deposition rates (Bojanowski et al., 2024). In these non-urban landscapes, the decomposition of plant biomass contributes to the formation of organic and inorganic nutrients. Moreover, land use affect hydrological processes, indirectly affecting nutrient transport pathways (Zhang et al., 2024). Forested and pasture areas typically exhibit higher infiltration rates and greater subsurface flow, which can reduce nutrient fluxes (Richards et al., 2021). In contrast, agricultural and urban landscapes are characterized by increased surface flow, leading to enhanced nutrient transport across the topsoil. Previous studies have established correlations between land use patterns and nutrient fluxes (Hamlin et al., 2020). For instance, forest cover is negatively associated with nutrient fluxes, while urban and agricultural areas show positive correlations (Jain et al., 2025). However, much of the existing research relies heavily on statistical analyses, leaving a process-based understanding of nutrient flux regulation across diverse landscapes insufficiently explored (Naden et al., 2016).

In this study, we combined observational data with the Export Coefficient Model (ECM) and the Soil and Water Assessment Tool (SWAT) to examine the variability of riverine nutrient fluxes in a typical urban agglomeration over the past 30 years. The specific objectives were to: 1) characterize the spatiotemporal patterns of nutrient fluxes, 2) assess the combined influences of hydrological processes, biogeochemical dynamics, and human activities, and 3) identify the key factors regulating each nutrient source.

2. Dataset and method

2.1. Study area

The Pearl River Delta (PRD) spans 55,400 km^2 and is located downstream of the Pearl River Basin (PRB) in southern China (Fig. 1). Urban land occupies approximately 10 % of the area, primarily around the coast of the Pearl River Estuary (PRE), while cropland in the central alluvial plain accounts for one-third of the delta. Forests dominate the periphery, covering over half of the PRD. The region experiences a subtropical oceanic climate characterized by abundant precipitation (exceeding 1500 mm per year), warm temperatures (averaging 22 °C), high solar radiation (5200 MJ/m^2 per year), and a dense river network (0.82 km/km^2). These conditions provide an optimal environment for agricultural activities and facilitate NPS nutrient transport.

The PRD consists of nine prefecture-level cities and is one of the most socioeconomically active regions in the world. This region experiences significant pollution from human activities, particularly near the coast and within the floodplain. By 2015, the PRD had become the world's largest urban agglomeration in terms of area and population (World Bank, 2015). This region generates over 80 % of Guangdong Province's GDP and is home to approximately 78.24 million people (Guangdong Statistical Bureau, 2020). Despite its impressive economic success, the degree of urbanization and industrial structure varies within this urban agglomeration. Furthermore, once known as the "world's factory floor", the PRD continually faces significant challenges in water quality degradation.

2.2. Model description

In this study, we simulated riverine nutrient fluxes of nitrogen and phosphorus by integrating the ECM with the SWAT model to account for point source (PS) and NPS nutrient contributions, respectively (Fig. 2). We achieved integration by incorporating PS data into the channel routing component of the SWAT model. We utilized the hydrology module of the SWAT, which has been thoroughly validated for the PRB, including climate forcing data, simulated streamflow (Fig. S1 in Appendix), and actual and potential evapotranspiration, as detailed in Zhang et al. (2024). Additionally, the nutrient module employed has been validated in nutrient fluxes and species throughout the Pearl River (Fig. S2 in Appendix). Furthermore, the ECM estimates annual nutrient inputs from PS based on the methodology outlined in the Manual of National Emission Source Census Pollutant Discharge Accounting Method and Coefficient (https://www.mee.gov.cn/). PS includes domestic discharges from both rural and urban areas, industrial wastewater, and contributions from the breeding industry, which encompasses livestock farming and aquaculture. Detailed parameters and equations related to PS in the ECM are provided in Text S1 in Appendix.

The SWAT model consists of two phases: the land phase and the stream phase. The land phase utilizes Hydrological Response Units as the computational units, which address landscape heterogeneity by integrating topography, soil properties, land use, and management practices (Bieger et al., 2019). The hydrological cycle is the primary driver of nutrients transport. The water balance is simplified as Equations (1) and (2):

$$Precipitation = AET + Runoff + Minor\ terms, \tag{1}$$

$$Runoff = Q_{sur} + Q_{lat} + Q_{aqu} \tag{2}$$

where AET represents actual evapotranspiration. Additional minor terms include re-evaporation from shallow aquifers to root zones, seepage from shallow aquifers to deep aquifers, and water storage in root zone and shallow aquifer. Q_{sur}, Q_{lat}, and Q_{aqu} denote surface, lateral, and aquifer flows, respectively. All terms are in millimeters (mm).

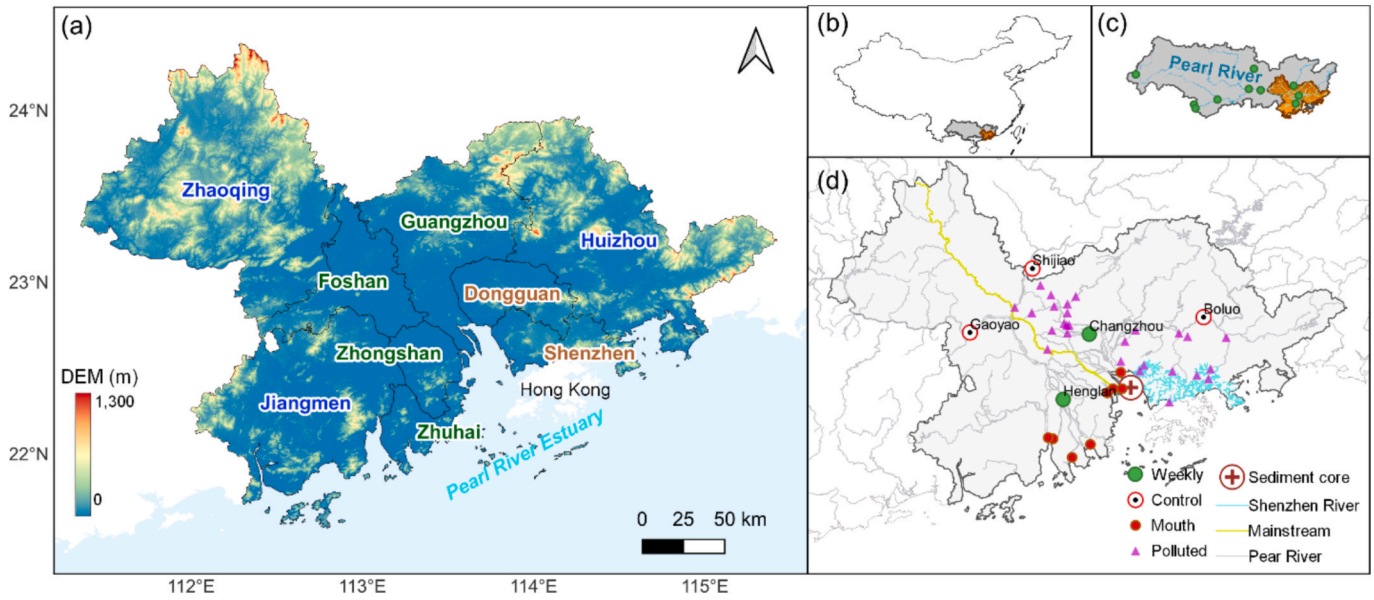

Fig. 1. (a) Land use and city distribution of the Pearl River Delta (PRD), (b) location of the Pearl River Basin (PRB) and (c) the PRD, and (d) observed nutrient stations.

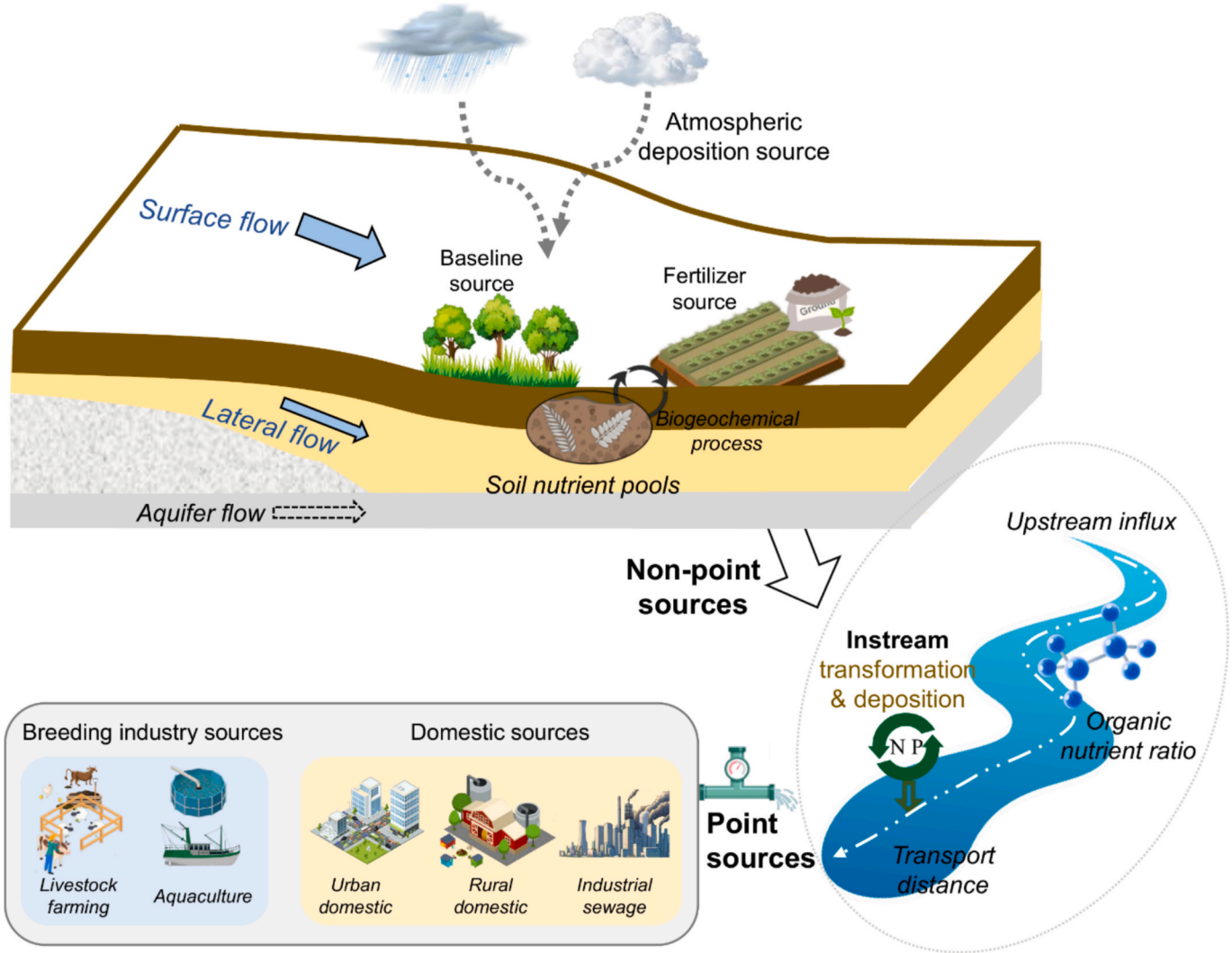

Fig. 2. Flowchart illustrating nutrient fluxes from various sources in the land phase and instream processes.

The SWAT model simulates NPS contributions from baseline conditions, nitrogen deposition, and fertilizer use (Fig. 2). Specifically, the baseline source reflects nutrient fluxes resulting from soil leaching in the absence of anthropogenic inputs, while the nitrogen deposition source accounts for contributions from both wet and dry deposition. The fertilizer source captures nutrient fluxes associated with crop cultivation. Nitrogen, with greater solubility and mobility than phosphorus, is transported through surface and lateral pathways, leading to its decomposition into surface and lateral components. In contrast, phosphorus tends to bind with soil particles and is mainly transported via surface flow (Nakayama et al., 2025). Soil biogeochemical processes are simulated to encompass fertilizer use, nitrogen deposition, denitrification, plant nutrient uptake, residue decomposition, and sorption–desorption reactions. The soil nitrate pool and the labile phosphorus pool are summarized in Equations (3) and (4):

$$\text{Nitrate pool} = \text{rsd}_{\text{nit}_n} + \text{act}_{\text{nit}_n}, \tag{3}$$

$$\text{Labile phosphorus pool} = \text{rsd}_{\text{laborg}_p} + \text{org}_{\text{lab}_p} - \text{lab}_{\text{min}_p} \tag{4}$$

where $\text{rsd}_{\text{nit}_n}$ represents nitrogen moving from fresh organic pool to nitrate pool, and $\text{act}_{\text{nit}_n}$ represents nitrogen transitioning from active organic pool to nitrate pool. Similarly, $\text{rsd}_{\text{laborg}_p}$ denotes phosphorus migrating from fresh organic pool to labile pool, $\text{org}_{\text{lab}_p}$ indicates phosphorus moving from organic pool to labile pool, and $\text{lab}_{\text{min}_p}$ represents phosphorus transitioning from labile mineral pool to active mineral pool. All terms are in kilograms per hectare (kg/ha). Detailed equations regarding nutrient transport in the land phase of the SWAT model are provided in Text S2 in Appendix.

Additionally, the stream phase simulates water and nutrient movements within channels (Fig. 2). The instream biogeochemical processes in the SWAT are based on the Enhanced Stream Water Quality Model (QUAL2E) (Brown and Barnwell, 1987). This module simulates algal growth, nutrient uptake by algae, transformations between organic and inorganic nutrients, and particulate deposition within the water column.

2.3. Model configuration

Tables 1 and 2 summarize the datasets used to set up the SWAT and ECM models for the PRD, respectively. For the SWAT model, geospatial data—including topography, soil, and land use—were employed for model initialization (Table 1). Besides, the river network was utilized to define channel routing and delineate watersheds. Meteorological data from the AgERA5 dataset, covering the period from 1979 to 2020 at a resolution of 0.1°, served as the atmospheric driver for the model.

Table 1
Datasets for setting up the Soil and Water Assessment Tool (SWAT) for the Pearl River Delta (PRD).

Category	Description	Temporal scale	Spatial scale	Source
Geography	Topography; soil	Static	1 km	National Cryosphere Desert Data Center (2025)
	River network	Static	50 *m*	
	Land use	Static	30 *m*	Zhang et al. (2021)
Atmospheric variables	Climate forcing	Daily	0.1°	Climate Data Store (2025)
	Wet and dry nitrogen deposition rates	Static	By land use	Yu et al. (2020)
Agronomy	Fertilizer applications	Annual	—	Statistics Bureau of Guangdong Province (2021)
	Tillage; crop rotation; irrigation; planting and harvesting dates	Static	—	

Table 2
Datasets for setting up the Export Coefficient Model (ECM) for the PRD.

Category	Description	Temporal scale	Spatial scale	Source
Social economy	Urban domestic water consumption	Annual	City	Water Resources Department of Guangdong Province (2021)
	Rural population	Decennial	County	National Bureau of Statistics (2021a)
	Industrial sewage discharge	Annual	City	National Bureau of Statistics (2021b)
	Livestock (intensive and free-range)	Annual	County	Statistics Bureau of Guangdong Province (2021)
	Aquaculture products	Annual	City	
Infrastructure	Urban domestic sewage collection rate	Annual	City	Statistics Bureau of Guangdong Province (2022)
	Proportion of administrative villages with rural sewage treatment	Annual	City	Department of Ecology and Environment of Guangdong Province (2024)
	Sewage treatment plant effluent concentration	Static	—	
Coefficients	Emission coefficients (livestock and aquaculture); removal rates (rural and urban domestic); per-capita rural pollutant intensity; water contamination factor; urban sewage concentration	Static	City	Ministry of Ecology and Environment (2021)

Agricultural practices were compiled from the Guangdong Agricultural Statistical Yearbook, while deposition rates were derived from the observation by Yu et al. (2020). To set up the ECM, socioeconomic factors and nutrient emission coefficients were compiled from various statistical yearbooks, bulletins, and manuals (Table 2).

Table 3 presents the datasets used for model validation, with the locations of the observation stations illustrated in Fig. 1d. Nutrient fluxes in the PRD were calculated by summing the nutrient outputs from eight outlets into the PRE and subtracting the total values from three upstream control stations in the PRD. Due to tidal influences, direct streamflow observations at the outlets were unavailable. Consequently, we estimated the streamflow for each outlet by multiplying the simulated basin-wide streamflow from Zhang et al. (2024) with the water distribution ratios in these outlets from Yao et al. (2009). Besides, since nutrient flux data from these stations were available only from 2018 to 2023, additional historical nutrient data were compiled from the literature. For nitrogen validation, historical ammonium concentrations were obtained from the China National Environmental Monitoring Centre for the period from 2004 to 2018. In the PRD, only two monitoring stations were available: Changzhou, representing the heavily polluted site, and Henglan, representing the less polluted site. For phosphorus validation, phosphorus concentrations from sediment cores near the outlet to the PRE covering 1990 to 2016 (Li et al., 2023), as well as phosphorus pollution indices for rivers in Shenzhen from 1991 to 2007 (Chen et al., 2011), were collected. Furthermore, to qualitatively validate the nutrient simulations, water quality data were collected from polluted rivers in the PRD for the period from 2014 to 2017, provided by the Department of Ecology and Environment of Guangdong Province.

Table 3
Datasets for model calibration and validation.

Category	Variable	Period	Data source
Hydrology	Streamflow at control stations	2018–2023	National Bureau of Statistics (2021c)
	Streamflow at outlets		Zhang et al. (2024)
Nutrient concentrations	Nitrogen and phosphorus concentrations at control stations and outlets	2018–2023	Department of Ecology and Environment of Guangdong Province (2024)
	Ammonium concentration	2004–2018	National Environmental Monitoring Centre (2019)
	Phosphorus concentrations in sediment cores	1990–2016	Li et al. (2023)
Water quality indicators	Phosphorus pollution index in Shenzhen rivers	1991–2007	Chen et al. (2011)
	Water quality in the Pearl River Basin	2014–2017	National Environmental Monitoring Centre (2019)
	Water quality in polluted rivers in the PRD	2004–2016	Department of Ecology and Environment of Guangdong Province (2024)

Additionally, data on the key section of water quality in the PRB covering 2004 to 2016 were sourced from the China National Environmental Monitoring Center.

Table 4 lists the key parameters used in the SWAT model. These parameters were initially calibrated during nutrient flux simulations for the PRB (Fig. S2 in Appendix), with several parameters subsequently adjusted to ensure an accurate representation of nutrient fluxes in the PRD.

2.4. Statistical analysis

Significant spatial variations in nutrient intensity were observed within the urban agglomeration. Based on the trajectories of diverse nutrient sources, we employed the *k*-medoids clustering algorithm (Meert et al., 2020) to classify cities and applied permutational multivariate analysis of variance (Rideout et al., 2023) to assess the statistical significance of the classification. The results reveal a core–periphery gradient comprising three distinct city types: domestic-heavy, hybrid-sourced, and agro-centric (Fig. S3 in Appendix). Domestic-heavy cities, including Shenzhen and Dongguan, are located on the eastern bank of the PRE (Fig. 1a). On the western bank, hybrid-sourced cities include Guangzhou, Foshan, Zhongshan, and Zhuhai. In contrast, agro-centric cities in the peripheral regions include Jiangmen, Huizhou, and Zhaoqing.

Nutrient fluxes from PS in the urban agglomeration exhibited an inverted U-shaped temporal pattern. We assessed the statistical significance of the regression coefficients using *t*-tests. The temporal pattern can be divided into three distinct stages: the initiation stage (1990), the peak stage (2002), and the protective stage (2020) (see Section 3.2.1). This pattern reflected a period of water quality degradation from 1990 to 2002, followed by a recovery period from 2002 to 2020. To capture this evolution, we calculated nutrient intensity for the three stages and analyzed the driving factors behind the changes during the two intervening periods. Additionally, we evaluated the contributions of various drivers to PS by differentiating the functions in the ECM model (Eqs. S1-11 in Appendix) with respect to these variables and multiplying by their corresponding values.

To compare the impact of different transport mediators and nutrient sources on nutrient flux, we min–max scaled their products. To further analyze the influence of land use on NPS, we calculated a variety of hydrological and biogeochemical factors, as well as the nutrient intensity for each land use type. Due to minimal sediment transport in the PRD, resulting from low erosion rates in the plain areas (Mu et al., 2022), the impacts of sediment on NPS were omitted from further analysis. The Redfield ratio describes the typical stoichiometric balance of essential elements in phytoplankton cells, with a common nitrogen-to-phosphorus (N:P) ratio of 16. When the N:P ratio exceeds 16, nitrogen is in surplus relative to phosphorus, and phytoplankton growth becomes constrained by phosphorus limitation (Ptacnik et al., 2010). The export-to-source ratio (η, dimensionless) of NPS pollution is defined in Equation (5):

$$\eta = N_{loss,\ i,\ j} / N_{source,\ i,\ j}, \tag{5}$$

where N_{loss} represents the nutrient loss intensity from the landscape (kg/ha), N_{source} denotes the nutrient source intensity (kg/ha). The subscript i refers to the nutrient species (e.g., surface nitrogen, lateral nitrogen, and phosphorus), while the subscript j indicates the specific source, such as fertilizer inputs, soil nutrient pools, or atmospheric deposition.

To investigate the key factors regulating instream processes (Fig. 2), we conducted a series of sensitivity tests. The baseline scenario involved the release of nutrients from PS in the upstream section of the mainstream (see Fig. 1d). To evaluate the effects of nutrient composition and transport distance, nutrients were released in varying ratios of organic to inorganic forms at different locations along the mainstream. Additionally, to account for the influence of upstream inflows, we coupled nutrient influx with the PRB at three control stations (i.e., Gaoyao,

Table 4
Calibrated parameters in the SWAT.

File	Parameter	Value	Description
hydrology.hyd	esco	0.65	Soil evaporation compensation factor
	epco	0.95	Plant water uptake compensation factor
	orgn_enrich	30,000	Organic N enrichment ratio
	orgp_enrich	1400 (1700*)	Organic P enrichment ratio
	cn3_swf	0.5	Soil water at cn3 (0 = fc; 0.99 = near saturation)
	bio_mix	0.5	Biological mixing efficiency
	perco	0.75	Percolation coefficient − adjusts soil moisture for percolation to occur (1.0 = fc)
	latq_co	30	Plant evapotranspiration curve number coefficient
nutrients.cha	ptln_stl	50	Organic N settling rate in reach
	ptlp_stl	1 (400*)	Organic P settling rate in reach
parameters.bsn	adj_pkrt_sed	0.1	Peak rate adjustment factor for sediment routing in the channel
	orgn_min	0.5	Rate factor for mineralization on active organic N
	n_uptake	5	Nitrogen uptake distribution parameter
	n_perc	3	Nitrate percolation coefficient (0–1) (0 = concentration of nitrate in surface runoff is zero; 1 = percolation has the same concentration of nitrate as surface runoff)
	p_perc	0.01	P percolation coefficient (0–1) (0 = concentration of soluble P in surface runoff is zero; 1 = percolate has the same concentration of soluble P as surface runoff)
	p_soil	1000 (2600*)	P soil partitioning coefficient
	p_avail	0.01	P availability index
	rsd_cover	2.00E-05	Residue cover factor for computing the fraction of cover

Note: The asterisk (*) indicates the raw parameter values used for the nutrient study in the Pearl River Basin.

Shijiao, and Boluo). Water influx scenarios were categorized into low, high, and realistic discharge levels, with low and high discharges set at 100 m^3/s and 10^9 m^3/s, respectively, while the realistic discharge was derived from our PRB model (Zhang et al., 2024). The removal ratio was calculated by dividing the total nutrient loss across channels by the total nutrient flux.

3. Results

3.1. Model performance

Fig. 3 compares the simulations for the PRD from 1990 to 2020 with reference datasets. The simulations revealed a decreasing trend in nutrient fluxes during 2016–2020, aligning well with observed trends during 2018–2023 (Fig. 3a). The underestimations of nitrogen and phosphorus by 8.2 % and 20.1 %, respectively, may be attributed to the limited response of the SWAT model to storm events. For nitrogen, the mean simulated ammonium concentration (0.64 mg/L) fell within the observed range at Changzhou (1.30 mg/L) and Henglan (0.22 mg/L) (Fig. 3b). The simulation also captured similar trends at these stations, with correlation coefficients (r) of 0.67 for Changzhou and 0.44 for Henglan. For phosphorus, the correlation between simulated fluxes in the PRD and concentrations derived from the sediment core yielded r = 0.47, showing a similar inverted U-shaped trend with peak values around 1996 to 2002 (Fig. 3c). Additionally, the correlation between simulated concentrations and the pollution index for Shenzhen rivers reached r = 0.64, with comparable peaks in the early 2000s (Fig. 3d). Moreover, the simulated nutrient fluxes showed strong consistency with water quality data from polluted rivers in the PRD, with correlations of r = 0.58 for nitrogen and r = 0.59 for phosphorus (Fig. 3e). Similarly, comparisons between simulated nutrient concentrations and observed overall water quality data from the PRB yielded high correlations of r = 0.74 for nitrogen and r = 0.70 for phosphorus (Fig. 3f). Overall, these comparisons suggested that the SWAT model performed reasonably well, supporting its reliability for process-based investigations into the spatiotemporal variability of nutrient fluxes and dynamics in the PRD.

3.2. Spatiotemporal characteristics

3.2.1. Long-term variation in source composition

Riverine nutrient fluxes in the PRD exhibited inverted U-shaped trajectories over the period 1990–2020, with significance levels of 95 % for nitrogen and 99 % for phosphorus (Fig. 4). These trajectories are characterized by an initial increase, a peak in 2002, and a subsequent decline, with final levels returning to those observed in 1990. During this study period, the average nutrient fluxes were 18.06 × 10^4 t/yr for nitrogen and 1.19 × 10^4 t/yr for phosphorus, resulting in a mean N:P ratio of 15.2. This ratio is close to the Redfield ratio of 16 and influenced by a high NPS ratio of 63.05 and a low PS ratio of 5.18. Nitrogen fluxes showed significant interannual variability, primarily driven by fluctuations in NPS, which contributed 44 % of the total nitrogen flux. In contrast, phosphorus exhibited greater overall variability than nitrogen due to the dominance of PS (nearly 90 %). Over the period, phosphorus levels fluctuated by approximately ±27 %, while nitrogen levels fluctuated slightly, by ±16 %.

The eight sources of nutrient fluxes displayed varying temporal patterns (Fig. 4). The urban domestic source consistently represented the largest contributor, accounting for approximately 31 % of nitrogen flux and 44 % of phosphorus flux. Only this source closely mirrored the overall trend of nutrient flux, initially increasing, peaking at 1.8 times its original level before declining by nearly 50 %. In contrast, the rural domestic source steadily declined, decreasing by more than half over the

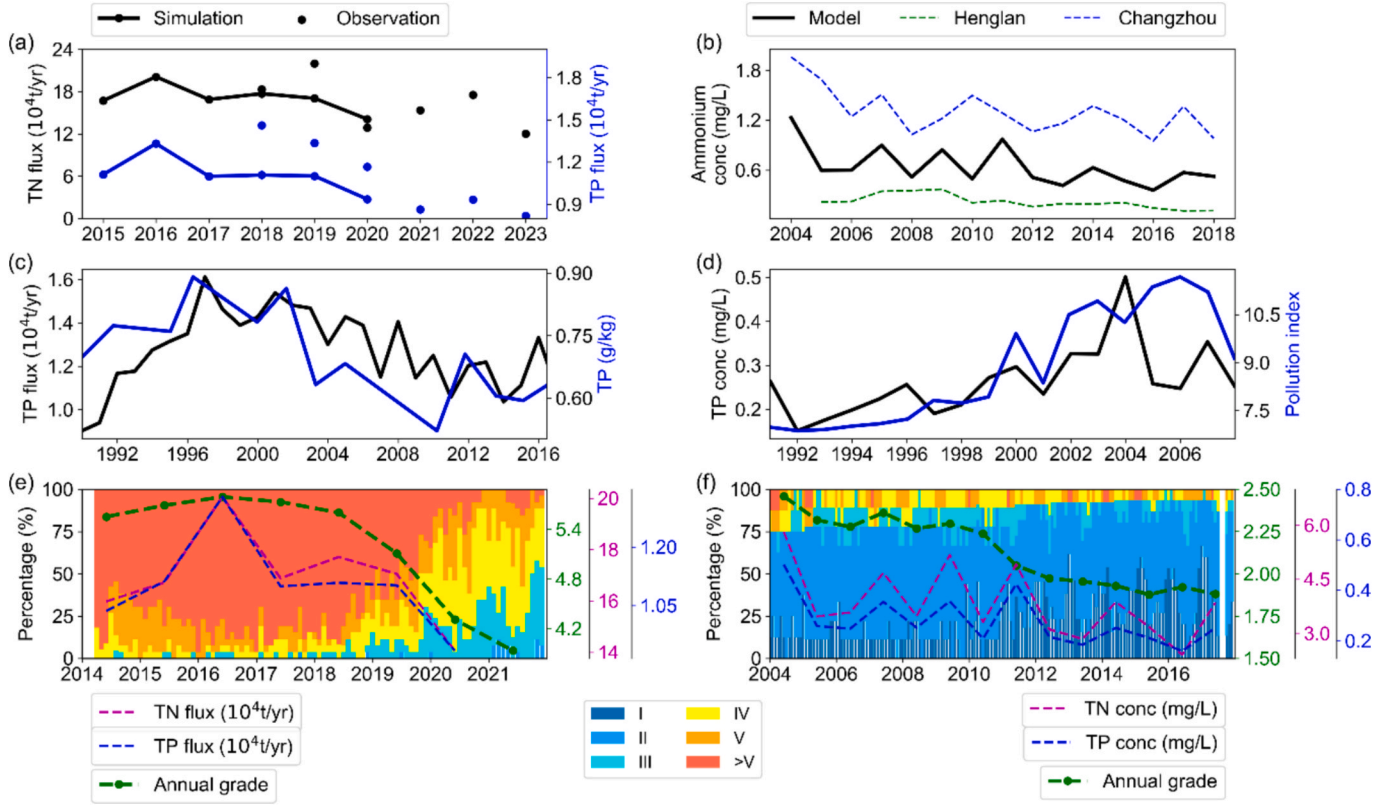

Fig. 3. Comparison of referenced and simulated data: (a) total nitrogen (TN) and total phosphorus (TP) fluxes; (b) ammonium concentration; (c) simulated TP flux from the PRD versus TP concentrations in sediment cores; (d) simulated TP concentration in the PRD compared to the TP pollution index in Shenzhen rivers; (e) simulated nutrient fluxes in the PRD versus water quality in polluted rivers within the PRD; and (f) simulated nutrient concentrations compared to water quality in the PRB.

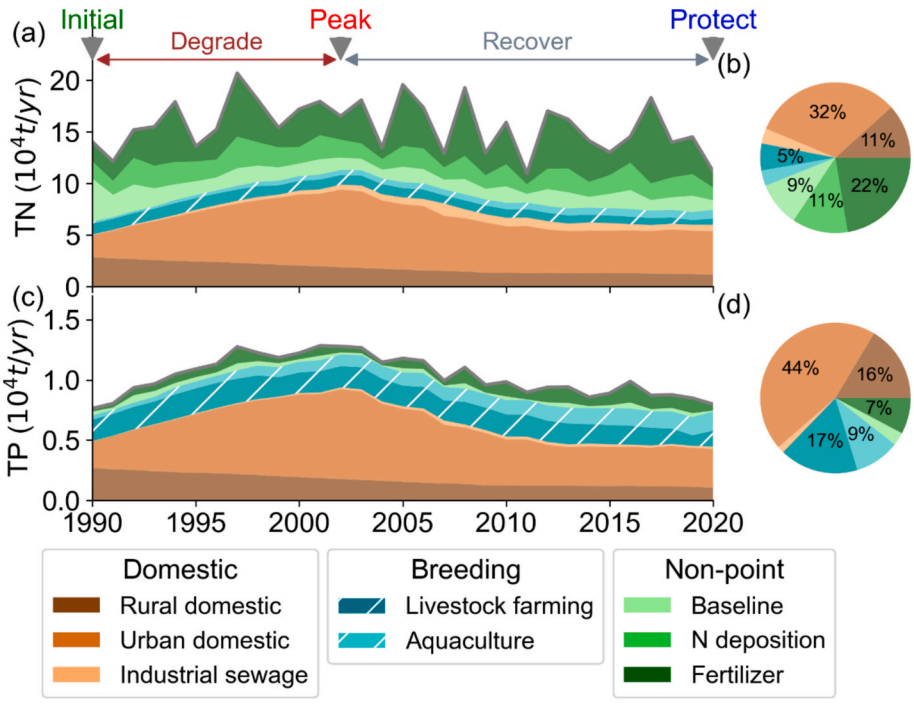

Fig. 4. Temporal dynamics of nutrient fluxes from various sources, along with pie charts for (a, b) TN and (c, d) TP. Key stages correspond to 1990 (initial), 2002 (peak), and 2020 (protective), while the intervening periods reflect phases of water quality degradation followed by recovery.

past three decades and contributing approximately 13 % of the total nutrient flux. Industrial wastewater, despite continuing to increase, contributed the smallest share of nutrients, accounting for only 2.5 % of the total flux. The breeding industry, encompassing livestock farming and aquaculture, showed contrasting trends that collectively resulted in a slight increase in nutrient fluxes. Specifically, nutrient flux from livestock farming steadily declined, decreasing by more than one-third between 1990 and 2020. In contrast, nutrient flux from aquaculture increased more than threefold during the same period, ultimately accounting for 16.6 % of the phosphorus flux by 2020. Among NPS, the contribution from fertilizer use was the largest (over 50 %). Nitrogen fluxes from baseline or nitrogen deposition sources were similar to those from rural domestic sources, with each contributing about 10 % of the total nitrogen flux, while their contributions to phosphorus were minimal.

3.2.2. *Spatially core-periphery structure*

Riverine nitrogen and phosphorus intensities among cities exhibited a strong correlation ($r = 0.97$), and the proportion of domestic sources also positively correlated with these intensities ($r = 0.94$) (Fig. 5). This spatial pattern supports a statistically significant core–periphery structure (*pseudo-F* = 8.25, $p = 0.01$), with intensity decreasing from domestic-heavy to hybrid-sourced and agro-centric city groups, extending from the eastern bank to the western bank and peripheral regions (Fig. S3 in Appendix). Specifically, Shenzhen and Dongguan were classified as domestic-heavy cities. These cities exhibited the highest nutrient intensities, with annual averages of 64.45 kg/ha for nitrogen and 4.53 kg/ha for phosphorus, and had the highest proportions of domestic sources, accounting for approximately 70.25 % of nitrogen and 90 % of phosphorus (Fig. 5). Notably, they had a high NPS of nitrogen, though the lowest NPS of phosphorus and breeding sources among city groups.

In contrast, Jiangmen, Zhaoqing, and Huizhou, situated in the

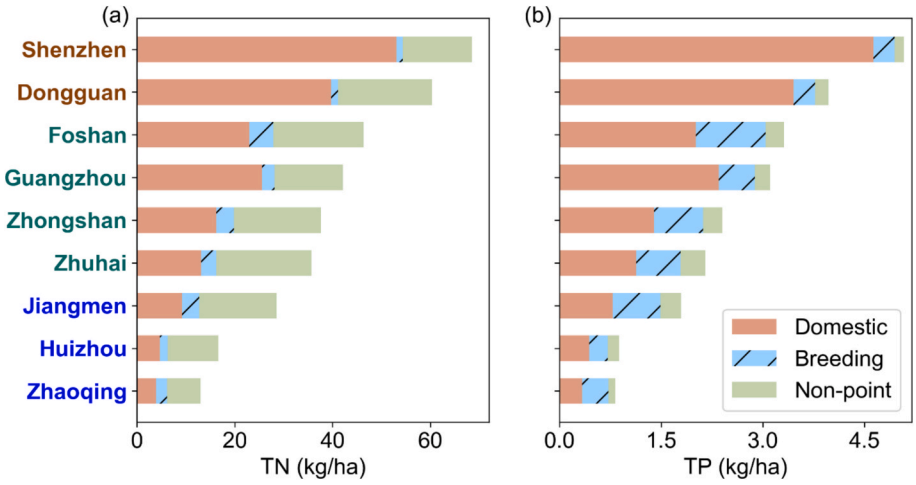

Fig. 5. Annual nutrient intensity of (a) TN and (b) TP at the city level.

periphery of the PRD, were classified as agro-centric cities. These cities had the lowest nutrient intensity levels, which were less than one-third of those in domestic-heavy cities. The agro-centric cities were predominantly influenced by non-domestic pollution, which accounted for 70 % of nitrogen and 56 % of phosphorus contributions. Guangzhou, Foshan, Zhongshan, and Zhuhai, located on the western bank of the PRE, were classified as hybrid-sourced cities. These cities exhibited intermediate levels of nutrient intensity and domestic source ratios (slightly exceeding 50 %), falling between those of domestic-heavy and agro-centric cities, with annual nitrogen intensity levels of 40.42 kg/ha and phosphorus intensity levels of 2.7 kg/ha. This group was characterized by the highest intensity of the non-domestic sources.

3.3. Controls on riverine nutrient flux

3.3.1. Land surface processes on NPS

To clarify the variability of NPS pollution in the study region, we analyzed its components from various sources across surface and lateral layers (Fig. 6). The active zone of NPS was primarily concentrated in the southwestern plain, where annual intensities of nitrogen and phosphorus reached 24 kg/ha and 0.32 kg/ha, respectively (Figs. 6a and 6g). Fertilizer sources dominated NPS pollution, contributing 55 % of the nitrogen and 74 % of the phosphorus (Figs. 6b and 6h). The active zones of baseline sources on the surface were scattered across the foothills surrounding the central alluvial plain, with nitrogen and phosphorus intensities of 1.6 kg/ha and 0.1 kg/ha annually, respectively—approximately four times higher than in surrounding areas (Figs. 6c and 6i). In contrast, the intensity of baseline nitrogen in the lateral layer was elevated, reaching an annual 4 kg/ha, and was extensively distributed across the southwestern and southeastern peripheral regions (Fig. 6d). The nitrogen deposition source exhibited divergent spatial patterns across the surface and lateral layers (Figs. 6e and 6f). In the surface layer, nitrogen deposition was most active in the central delta near the PRE, with annual intensities exceeding 8 kg/ha, followed by surrounding areas at approximately 4 kg/ha. Conversely, in the lateral layer, nitrogen deposition was most active in the northeastern periphery, with an annual intensity of 3.2 kg/ha. Overall, these similarities and differences in distributions suggest both shared and distinct mechanisms among NPS categories.

We then further investigated the characteristics of hydrological and biogeochemical factors that regulate NPS pollution on the land surface (Fig. 7). Surface flow was most active in the central delta, with moderate activity in surrounding areas, aligning with the spatial distribution of surface-layer nitrogen deposition sources (r = 0.87) (Figs. 6 and 7). Lateral flow, nitrogen deposition rates, and nitrogen pools from nitrogen deposition were most active in the northeastern peripheral regions, corresponding to the lateral-layer nitrogen distribution from nitrogen deposition sources (r = 0.77). In contrast, baseline soil nutrient pools were concentrated in the southwestern and southeastern peripheral regions, consistent with the lateral-layer distribution of baseline nitrogen sources. Fertilizer use was particularly high in the southwestern plain. However, only 1/158 of phosphorus fertilizer and 1/5 of nitrogen fertilizer were transported into rivers, resulting in a high N:P ratio of 68 for fertilizer sources.

Land use directly influenced hydrological and biogeochemical processes on the land surface (Fig. 8). It controlled flow components, with elevated surface flow (over 1,000 mm/yr) in urban areas located in the center of the PRD (Figs. 7 and 8). Agricultural land within the alluvial plains experienced intensive fertilizer use (144 kg/ha of nitrogen and 65 kg/ha of phosphorus annually) and moderate surface flow (432 mm/yr). In contrast, lateral flow was most pronounced in forested regions, reaching up to 900 mm/yr. Forests also acted as active zones for soil nutrients, providing abundant annual nitrate (128.6 kg/ha) and labile phosphorus (20.3 kg/ha) pools from baseline sources attributed to extensive organic residue accumulation. Additionally, forests exhibited elevated nitrogen deposition rates (36.6 kg/ha annually), 1.3 times higher than those in urban and agricultural areas, contributing to a high nitrate pool at an annual intensity of 30.5 kg/ha.

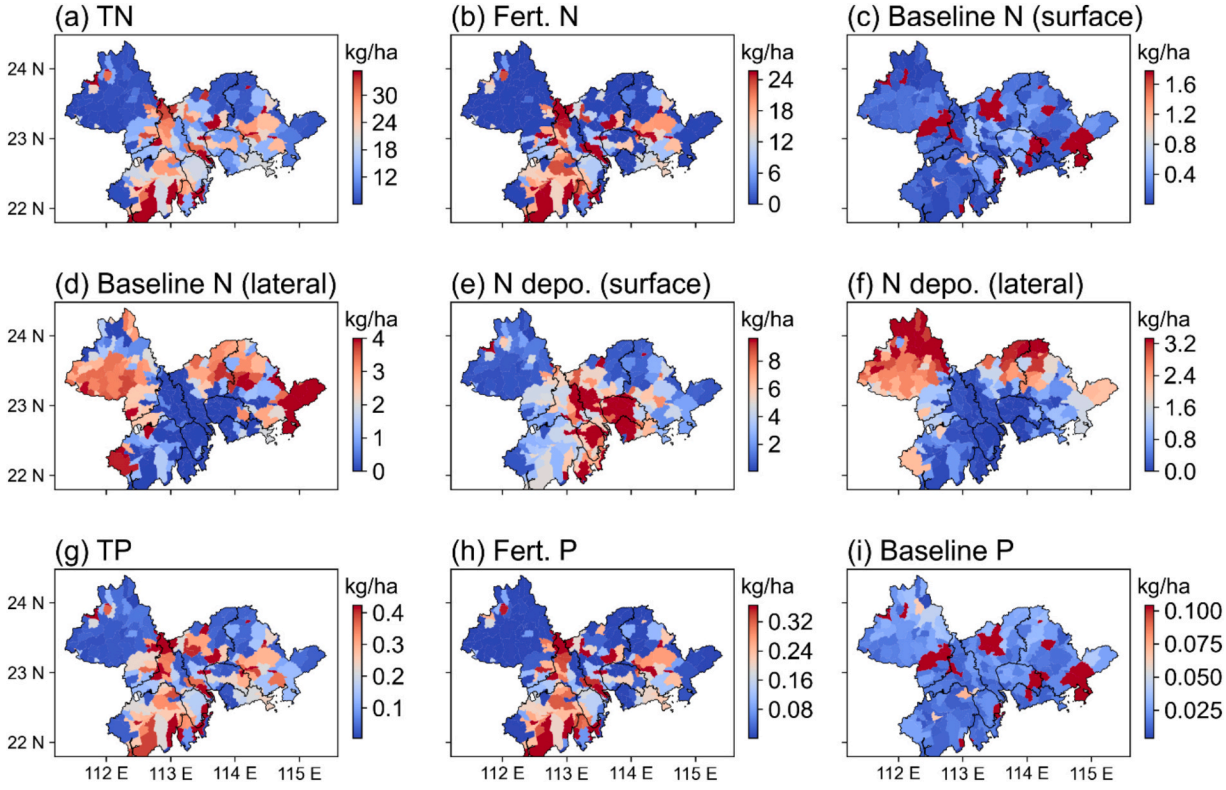

Fig. 6. Annual nutrient intensity of non-point sources (NPS) and its components: (a) nitrogen, which includes (b) fertilizer sources; baseline sources of (c) surface and (d) lateral layers; and nitrogen deposition sources of (e) surface and (f) lateral layers; and (g) phosphorus, which includes (h) fertilizer sources and (i) baseline source.

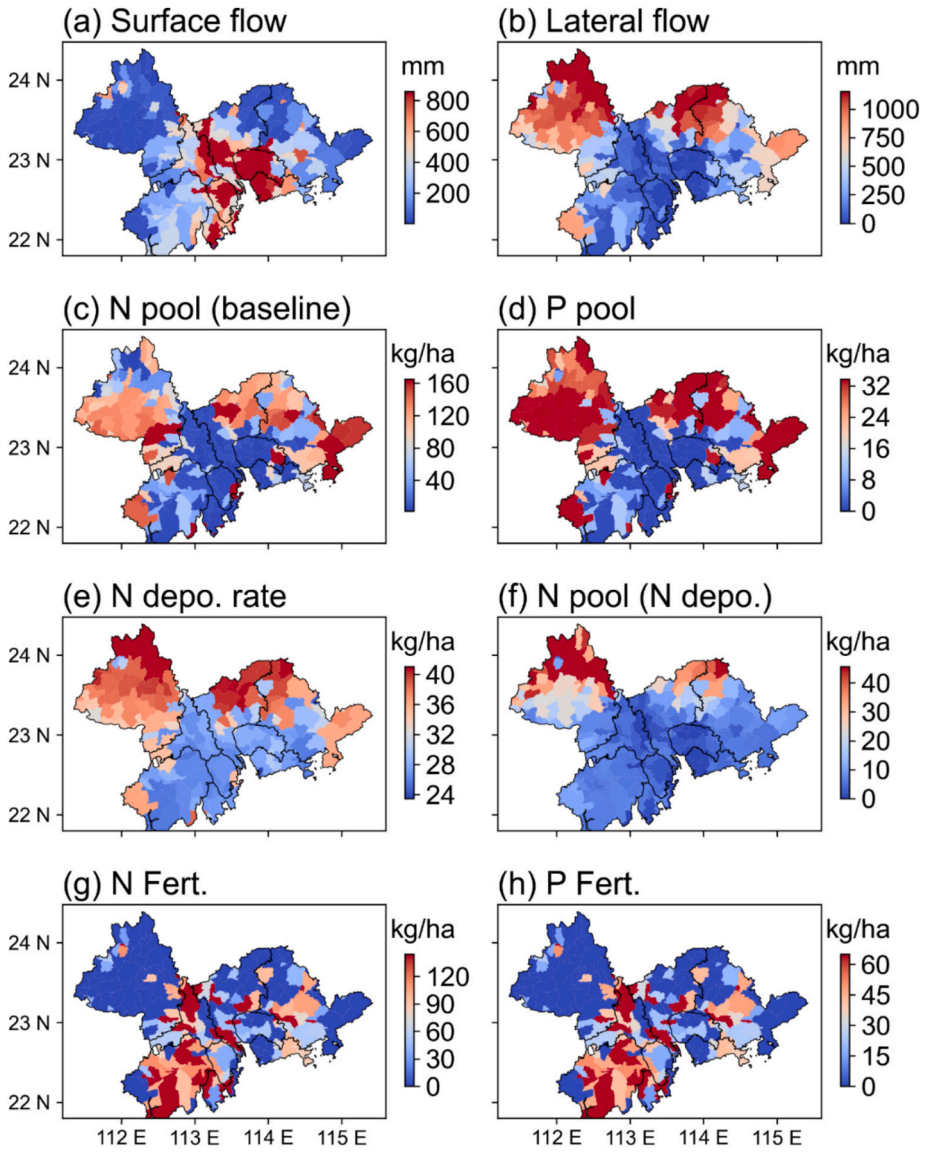

Fig. 7. Annual intensity of factors impacting nutrient flux: (a) surface flow, (b) lateral flow, (c) soil nitrate pool (N pool) from baseline sources, (d) soil labile phosphorus pool (P pool), (e) nitrogen deposition rate, (f) N pool from nitrogen deposition, (g) nitrogen and (h) phosphorus fertilizer use.

We quantified the relationships between NPS categories and their controlling factors and compared nutrient intensity across different land uses (Fig. 9). Nutrient dynamics were proportional to the coupling of transport processes and nutrient inputs, with all r values being higher than 0.85. Surface flow played a dominant role in nutrient transport in the PRD by actively coupling inputs from fertilizer, atmospheric deposition, and soil nutrients; these couplings created distinct active zones for NPS components (Figs. 7 and 9). Specifically, agricultural land exhibited the highest annual nutrient yield, at 25.16 kg/ha for surface nitrogen and 0.37 kg/ha for phosphorus, as surface flow interacts with intensive fertilizer use. Surface flow also interacts with atmospheric deposition, which regulates nitrogen deposition sources in the surface layer. Annual nutrient contributions from this source are most pronounced in urban areas (11.23 kg/ha) and agricultural areas (5 kg/ha), compared to forested areas (1.18 kg/ha). This contrasts with the pattern of nitrogen deposition rates, highlighting the dominant role of surface flow in nutrient transport from atmospheric deposition (Figs. 8 and 9). In addition, surface flow interacted with soil pools, which regulate baseline levels of surface nitrogen and phosphorus. However, baseline nutrient intensity is lower compared to other sources due to the limited overlap between active soil nutrients and surface flow (Figs. 7 and 9). For example, forests exhibit the highest baseline nutrient levels, at 1.13 kg/ha of nitrogen and 0.06 kg/ha of phosphorus annually, due to their high soil nutrient content; however, these levels are constrained by low surface flow.

Forested regions displayed elevated annual nitrogen levels (5.7 kg/ha) in the lateral layer, which were higher than its nitrogen intensity in the surface layer (1.3 kg/ha) (Figs. 9a and 9b). The soil nitrogen pool played a key role in regulating both baseline and nitrogen deposition sources in the lateral layer ($r > 0.85$) (Fig. 9b). In contrast to the significant role of surface flow, lateral flow did not notably limit nutrient fluxes in this layer. Nitrogen was more readily transported than phosphorus, with its export-to-source ratio η being much greater than 1 %. For nitrogen, surface flow demonstrates a high transport capacity, with η exceeding 13 % for sources from nitrogen deposition and fertilizer use, compared to over 5 % from soil pools. Overall, these relationships indicate that land use regulates nutrient components by influencing hydrological and biogeochemical processes. The rationale for this mechanism is discussed in Section 4.1.

3.3.2. *Human activities on PS*

To understand the evolution of nutrients resulting from human

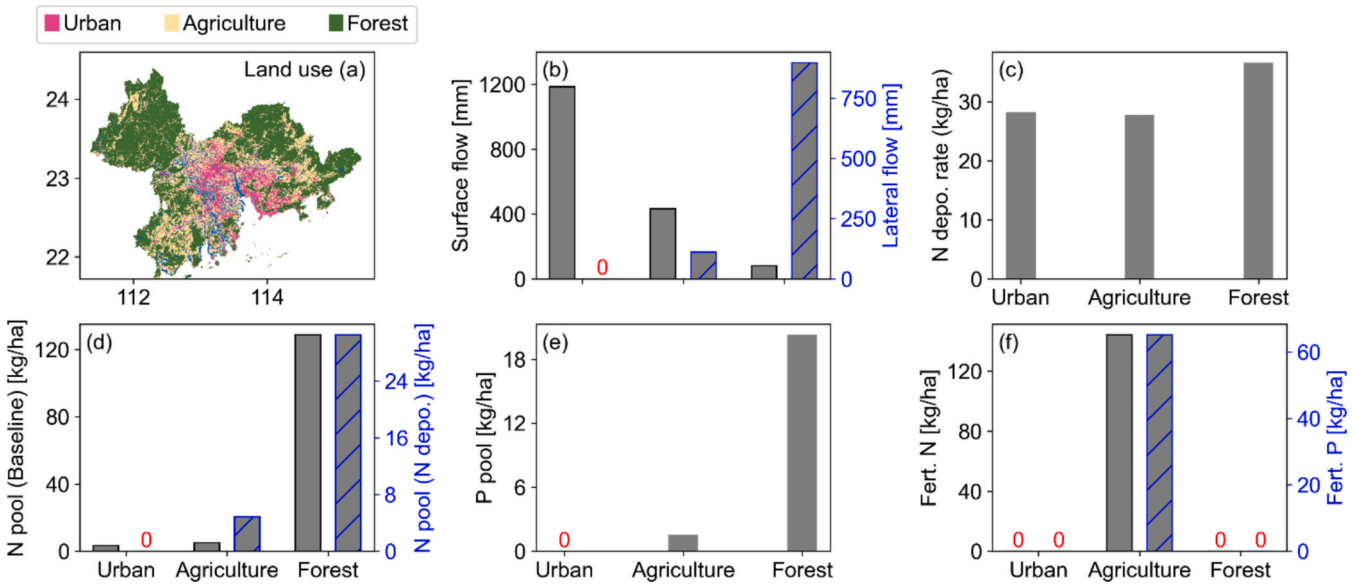

Fig. 8. Maps of (a) land use and factors impacting nutrient flux across different land uses of (b) surface flow and lateral flow, (c) nitrogen deposition rate, (d) N pool from baseline and nitrogen deposition, (e) P pool, and (f) nitrogen and phosphorus fertilizer use.

activities, we analyzed the intensity of PS categories across three temporal stages of the U-shape curve in the domestic-heavy, hybrid-sourced and agro-centric source cities, and examined the contributions of a variety of factors during the two intervening periods (Fig. 10). The core-periphery pollution structure remained consistent throughout all stages. The contributions of factors exhibited consistent directional trends across city groups, reflecting the integrated nature of the PRD agglomeration.

As urbanization progressed, urban domestic sources sharply increased due to rising water consumption during the degradation stage, followed by a decline resulting from improvements in wastewater treatment during the recovery stage (Fig. 10). Rural domestic sources continuously decreased, initially due to a declining rural population and later due to improvements in rural wastewater treatment. Nutrient flux from the breeding industry experienced a slight increase with agricultural modernization, driven by contrasting trends in livestock farming and aquaculture. The reduction in livestock farming was primarily attributed to a higher proportion of intensive farming practices, while the expansion of aquaculture was mainly linked to freshwater fish farming.

The evolution of nutrient emissions varied among city groups, driven by distinct source compositions. Domestic-heavy cities maintained the highest nutrient intensity and exhibited the most pronounced temporal variations, largely due to the dominance of urban domestic sources, which accounted for over 90 % after the peak stage (Figs. 10a and 10d). Urban domestic sources increased more than tenfold from the initial to the peak stage, followed by a 40 % decline by the protective stage. In contrast, nutrient flux from the breeding industry decreased by 80 % during the protective stage, due to a high ratio of intensive farming practices.

Hybrid-sourced cities exhibited similar trends to domestic-heavy cities in urban domestic sources, tripling during the degradation period and then decreasing by nearly half during the recovery period (Figs. 10b and 10e). Conversely, breeding industry sources continued to rise, driven by increases in freshwater aquaculture, reflecting a transition from livestock farming dominance to aquaculture dominance.

Agro-centric cities exhibited the lowest nutrient intensity from PS, showing the greatest disparity during the peak stage compared to other city groups, at approximately one-eighth of that of domestic-heavy cities and one-quarter of hybrid-sourced cities (Figs. 10c and 10f). Nutrient intensity remained relatively stable, with domestic sources annually averaging approximately 5.3 ± 1 kg/ha and breeding industry sources around 2.4 ± 0.3 kg/ha. Urban and rural domestic sources were comparable after the peak stage and experienced synchronous decreases, while livestock farming remained the dominant source within the breeding industry, albeit at a declining trend. Overall, these similarities and differences among city groups in nutrient evolution suggest a division of labor and cooperation within the urban agglomeration. Potential explanations for these patterns are discussed in Section 4.2.

3.3.3. *Instream process*

We examined the key factors regulating instream biogeochemical processes: organic nutrient ratio, transport distance, and upstream influx from the PRB (Fig. 11). The organic nutrient ratio had the greatest influence on nutrient loss (Figs. 11a and 11d). Nitrogen exhibited a particularly strong response to this ratio, with an organic-only scenario resulting in a nitrogen loss ratio of 20.5 %, which was over five times greater than the phosphorus loss. Conversely, the total transformation of nitrogen species was negatively correlated with this ratio, as transformation was dominated by inorganic forms.

Transport distance over the river networks positively influenced instream nutrient transformation and removal across all species (Figs. 11b and 11e). For instance, a transport distance of approximately 400 km, from the upstream reaches of the PRD to the estuarine outlet, resulted in a 9.2 % loss of nitrogen and a 2.8 % loss of phosphorus—three times greater than the losses observed over a 100 km travel distance.

Furthermore, the actual influx from the PRB did not significantly affect the local nutrient transformation loads within the PRD (Figs. 11c and 11f). Instead, the high nutrient concentration in low streamflow scenarios, compared to the reality scenario, accelerated nutrient transformation and doubled the nutrient removal rate. In contrast, the dilution effect of high streamflow scenarios had a minimal impact on nutrient dynamics.

Overall, the magnitude of nitrogen transformation and removal was significantly greater than that of phosphorus. For nitrogen, the deposition of organic nitrogen emerged as the dominant pathway contributing to nitrogen loss as ammonium was primarily converted into nitrite (Fig. 11a–c). For phosphorus, both organic and inorganic forms substantially contributed to nutrient loss, which may be through adsorption onto sediments followed by deposition in the water column (Fig. 11d–f).

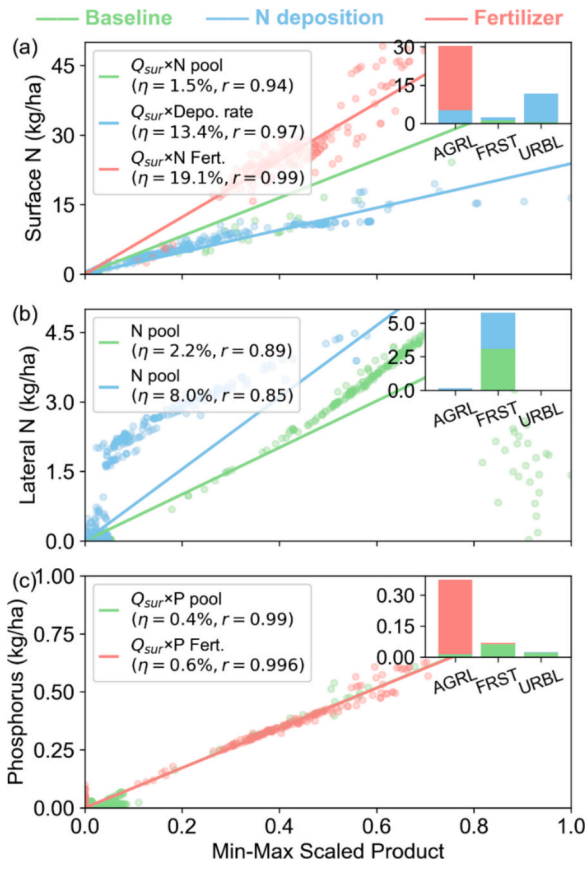

Fig. 9. Nutrient species controlled by the coupling of transport mediators and nutrient sources, including (a) nitrogen in the surface layer, (b) nitrogen in the lateral layer, and (c) phosphorus. The *x*-axis shows the min–max scaled product of the transport mediators and nutrient sources, and the *y*-axis represents the intensity of nutrient species. The inset axis displays nutrient intensity across different land uses, including AGRL (agriculture), FRST (forest), and URBL (urban). The controlling factors for each species and source, with the nutrient transport efficiency (η) and correlation coefficients (r), are annotated. Green, blue, and red lines represent regression lines for baseline, nitrogen deposition, and fertilizer sources, respectively. (For interpretation of the references to colour in this figure legend, the reader is referred to the web version of this article.)

4. Discussion

4.1. NPS controlled by hydrological and biogeochemical processes

In this study, we systematically investigated and differentiated the components of NPS pollution across various land uses regulated by hydrological and biogeochemical processes. Agricultural regions are recognized as hotspots of NPS pollution due to the concentrated accumulation of fertilizers in the topsoil, which significantly contributes to widespread eutrophication and estuarine hypoxia (Han et al., 2023). This issue is further exacerbated by enhanced surface flow (Fig. 8) resulting from soil compaction caused by intensive tillage and heavy machinery use. The active interaction between fertilizer uses and surface flow (Fig. 9) facilitates rapid and high ratio of nutrient exports, especially in regions with monsoonal or high-intensity rainfall patterns. Notably, nitrogen fertilizers exhibit a significantly higher proportional transport into riverine systems compared to phosphorus fertilizers (Fig. 9), as phosphorus tends to adsorb strongly to soil particles due to the chemical affinity of phosphate ions for iron oxides and other mineral surfaces (Basinski et al., 2024). As shown evidently in this study, these processes lead to elevated N:P ratios in NPS pollution and chronic nitrogen exceedances in river networks, a phenomenon commonly observed in agricultural watersheds. Moreover, the relatively low N:P ratio from PS shifts the overall ratio in the PRD toward the Redfield benchmark, thereby facilitating phytoplankton growth and increasing the risk of algal blooms. Therefore, water managers should adopt dual nutrient management strategies that address nitrogen and phosphorus simultaneously in the urban agglomeration.

Surface flow also plays an important role in transporting nutrients from baseline and atmospheric deposition sources in surface layers (Fig. 9). Nutrients from baseline sources are primarily observed in areas where high surface flow overlaps with soil nutrients in foothill regions (Figs. 6 and 7). This overlap produces a scattered spatial distribution of nutrients, attributable to heterogeneous topography and patchy distributions of vegetation and organic residues. Regarding nitrogen deposition sources, urban areas are major contributors due to prevalence of surface flow on impervious surfaces, which inhibit soil infiltration (Zhang et al., 2024). Additionally, atmospheric deposition rates in the PRD exceed those observed in North America and Europe by two to threefold, primarily driven by local fossil fuel combustion and fertilizer volatilization, leading to intensified nitrogen fluxes (Nespoulous et al., 2019). To address elevated nutrient fluxes from NPS pollution, China launched source mitigation measures, such as the "Battle Against Agricultural Non-Point Source Pollution" in 2015 and a zero-growth plan for chemical fertilizer use (Tables S1 and S2 in Appendix). However, mitigation measures on transport process are critical in both agricultural and urban landscapes (Hoffmann et al., 2020). Among surface flow interception strategies, the relative cost typically decreases in the sequence of constructed wetlands, storage ponds, and riparian buffers (Cole et al., 2020; Walton et al., 2020). It is important to note that best management practices are site-specific and should be scientifically tested, considering environmental benefits, costs, and practical feasibility (Luna Juncal et al., 2023).

Nutrient fluxes from lateral flow merit significant attention, particularly within forested areas that encompass over half of the study region (Figs. 6 and 8). The pronounced lateral nutrient fluxes in forested ecosystems arise from elevated soil nutrient pools combined with enhanced lateral flow dynamics (Figs. 8 and 9), supporting that lateral flow is not a limiting factor in nutrient transport (Mihiranga et al., 2022). The substantial soil nutrient pools result from active microbial decomposition of organic debris under subtropical and tropical climates, releasing bioavailable nutrients predominantly stored in subsurface soil horizons (Chen et al., 2025). Enhanced lateral flow is facilitated by high canopy interception in forests, elevated hydraulic conductivity, and well-connected macropore networks in humid forest soils. Additionally, the mountainous terrain increases lateral hydraulic conductivity by several folds compared to flat landscapes (Lu et al., 2024). To mitigate lateral nutrient fluxes, root-mediated interventions targeting nutrient uptake are particularly effective. The overall feasibility of such interventions decreases from managing root density to cultivating deep-rooted species (Li et al., 2025; Zeng et al., 2020). Moreover, these approaches contribute to long-term soil fertility, enhance forest productivity, and promote biodiversity.

4.2. Controls on spatiotemporal patterns of riverine nutrients

Although the trends of different sources in PS nutrient fluxes vary (Fig. 4), their temporal variations are primarily influenced by economic development and environmental protection policies. Among the PS categories, urban domestic sources uniquely exhibit a trend consistent with the EKC, which reflects an early emphasis on economic growth, which later shifted toward environmental protection. During initial economic expansion, labor-intensive manufacturing drove rapid population growth and increased urban water consumption (Cheung and Leung, 2018). However, effective pollution control measures were delayed until the introduction of the "Total Pollutant Control Plan" in 1996, which aimed to curb pollutant emissions and peaked in nutrient fluxes in the early 2000s (Tables S1 and S2 in Appendix). Subsequently,

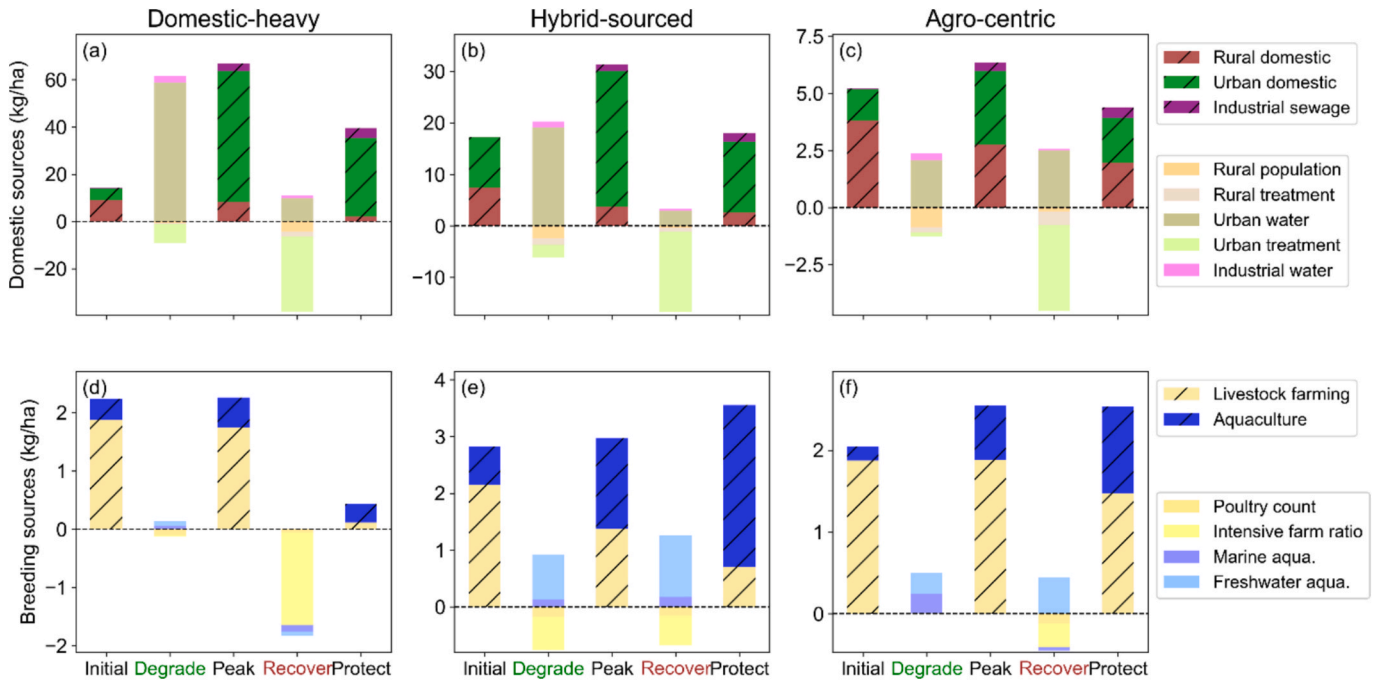

Fig. 10. Annual nutrient intensity and factors impact on changes for TN (upper panels) and TP (lower panels) across city groups: (a, d) domestic-heavy cities, (b, e) hybrid-sourced cities, and (c, f) agro-centric cities.

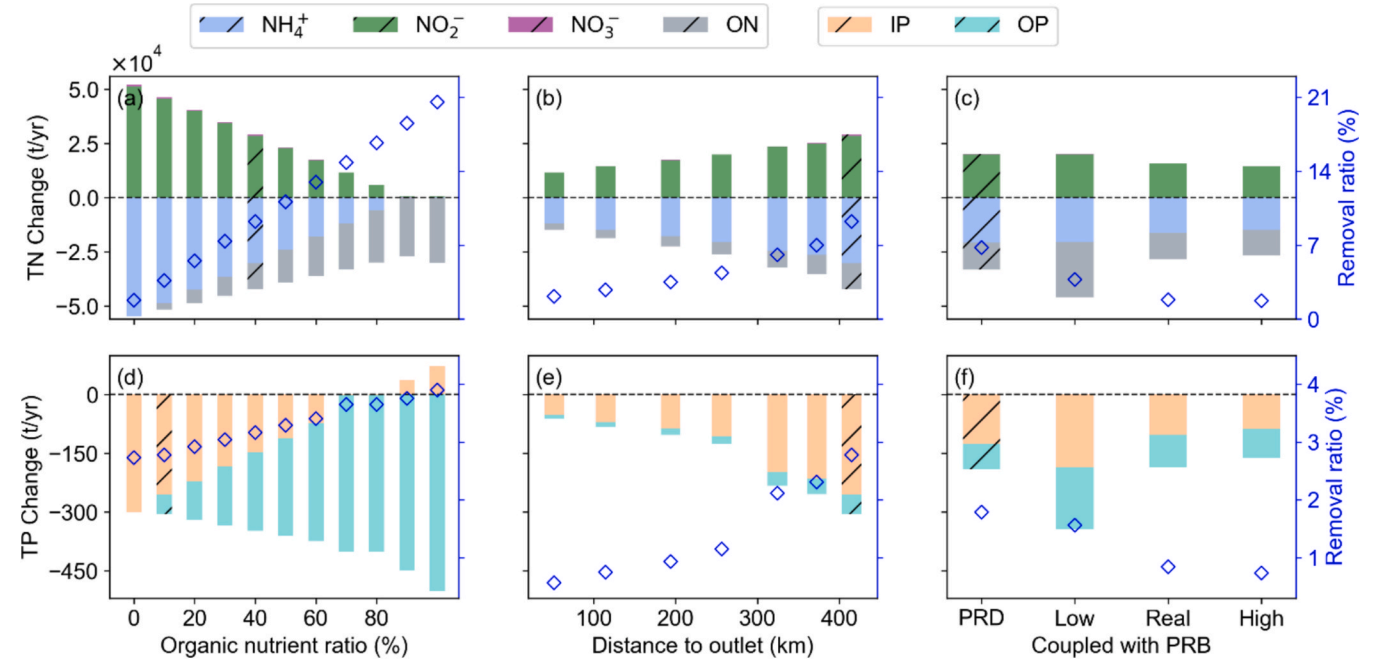

Fig. 11. Instream biogeochemical processes: TN (upper panels) and TP (lower panels) transformations (bar plots) and removal ratios (scatter plots), showing (a, d) variation with organic matter ratios, (b, e) variation with distance to the outlet, and (c, f) coupling with the PRB under low, high, and realistic discharge scenarios.

as economic priorities shifted toward environmental protection, particularly following the State Council's introduction of comprehensive reforms and targeted pollution control measures in 2011. The PRD, like many other rapidly developing regions, has transitioned toward an innovative-driven economy, with the tertiary sector emerging as the dominant economic force during the protective stage. As a result, wastewater treatment infrastructure has improved significantly, reaching levels comparable to those of developed countries, with current treatment rates exceeding 90 % in both urban and rural areas (Tang et al., 2022).

In contrast to urban domestic sources, other nutrient sources exhibit trends that deviate from the EKC model (Fig. 4) due to complex interplay between economic growth and environmental protection. For example, nutrient fluxes from rural domestic sources have declined, largely driven by urbanization-induced population migration and improvements in rural wastewater treatment systems. Similarly, livestock farming has decreased (Fig. 10), as poultry and livestock production have been relocated to surrounding cities of the PRD, such as Shaoguan and

Qingyuan, where greater land availability supports more efficient farming practices. This relocation, combined with a shift toward intensive farming systems, has contributed to the reduction in livestock-related nutrient fluxes. In contrast, nutrient fluxes from industrial sewage and aquaculture display consistent increases, primarily driven by ongoing economic growth. For instance, the expansion of aquaculture has been fueled by the growing demand for diversified food systems that prioritize high-quality protein sources (Bao et al., 2019).

Urban agglomeration exhibits an integrated spatial structure, reflected in similar trends in domestic nutrient sources and consistent directional trends in key influencing factors across city groups (Fig. 10). This integration is further reinforced by the region's political framework (Tables S1 and S2 in Appendix). Notably, the conceptualization of the PRD as an urban agglomeration was first introduced in 1994 and later solidified by the national-level strategic plan in 2019, "Outline Development Plan for the Guangdong-Hong Kong-Macao Greater Bay Area" (The State Council of the People's Republic of China, 2019).

Despite this integration, non-domestic sources have led to divergent trends among different city groups (Fig. 10). Their fluxes in domestic-heavy cities continue to decline, driven by the steady expansion of the environmentally friendly tertiary sector, which accounted for over 50 % of the regional economy during the protective stage (Guangdong Statistical Bureau, 2020). Additionally, rapid urban expansion has displaced agricultural activities in these cities, contributing to a downward trend in non-domestic pollution (Liu et al., 2018). However, nitrogen deposition has emerged as the dominant NPS of pollution in domestic-heavy cities, primarily due to high surface flow over impervious surfaces (Figs. 6 and 7).

In contrast, agro-centric cities face challenges in reducing non-domestic sources of nutrient flux. Agriculture remains a key industry in these areas, driven by the need to meet the growing food demands of accelerated urbanization. For instance, Jiangmen, one of the region's primary agricultural zones, generates substantial pollution due to intensive fertilizer use (Figs. 5 and 6). Additionally, nutrient fluxes from industrial sewage have slightly increased since the implementation of Guangdong Province's "Double Transfer" strategy in 2008, which relocated labor-intensive industries from the central delta to peripheral areas (Cheung and Leung, 2018). Furthermore, weaker environmental regulations in remote regions have contributed to persistently high levels of nutrients.

Hybrid-sourced cities are emerging as pollution hotspots due to their dual reliance on domestic and non-domestic sources. On one hand, these cities share similarities with domestic-heavy cities, as they were the pioneers of China's reform and opening-up policies, leading to significant contributions from domestic nutrient sources. On the other hand, they also generate the region's highest levels of non-domestic pollution (Fig. 5), corresponding to their strong GDP contributions from the primary sector. The predominant land uses in these cities—cropland and urban areas—act as active zones of nutrient fluxes, with fertilizers and nitrogen deposition significantly contributing to NPS pollution (Fig. 8). Additionally, the dense river network in delta and proximity to estuaries have facilitated extensive aquaculture, which now accounts for 68 % of Guangdong Province's total output (Liu et al., 2018).

4.3. Limitations and perspectives

Our study investigates long-term riverine nutrient dynamics and pathways within a coupled human-hydrological-biogeochemical framework. Like all other similar studies, the limitations of the current study exist, such as contributions to riverine nutrient loads from groundwater. However, this contribution is expected to be minor in the PRD, as groundwater accounts for less than 10 % of total runoff (Fig. S4 in Appendix). The groundwater-borne nitrogen in the PRD primarily originates from domestic and industrial sewage (Huang et al., 2021), and we have accounted for these sources in the ECM. The coupling between the SWAT with 3D groundwater flow models and reactive transport models requires extensive observation datasets and further investigation (Yang et al., 2024).

The temporal resolution of our analysis is constrained by the ECM module, which operates at an annual scale and does not capture seasonal variability in PS. Furthermore, several parameters are treated as static (Table 2)—for example, removal rates for rural and urban domestic pollutants and pollutant production intensities—based on available statistics due to spatiotemporal limitation of observational data. Finally, our analysis focuses on long-term variations in nitrogen and phosphorus, while the detailed speciation of nutrients from NPS and PS remains for future work. Improvements in land use classification and management practices are also warranted, as plant and crop types differ in their interactions with nutrients and soils.

Further improvements to the model and observation network pose a great challenge in capturing the large-scale pollutant flux across the global river basins. Emerging artificial intelligence approaches may address these challenges by providing continuous, spatiotemporal, multi-indicator assessments of water quality across diverse landscapes (Ismail et al., 2024; Kieu and Quoc, 2024). Such developments would enable a more nuanced understanding of nutrient dynamics and support targeted management strategies.

5. Conclusions

This study elucidates the dynamics of riverine nutrient fluxes and their pathways within a coupled human-hydrological-biogeochemical framework by examining a typical urban agglomeration during a period of rapid socioeconomic development. The following conclusions can be drawn from the analysis:

1. Nutrient dynamics of NPS are proportional to the coupling of transport processes and nutrient inputs. Surface flow is particularly high in urban and agricultural areas, making agricultural land an active NPS zone due to the intensive fertilizer use, while urban areas serve as hotspots for surface nitrogen transport from nitrogen deposition. High nitrogen levels in forested regions result from soil nitrate pool in the lateral layer, where lateral flow is not a limiting factor.
2. PS variations are primarily driven by domestic sources, which initially surged and subsequently declined following significant advancements in wastewater treatment. Domestic sources establish a core-periphery pollution structure, where intensity decreases from domestic-heavy and hybrid-sourced areas at the core to agro-centric regions at the periphery. However, this structure weakens as domestic sources decline significantly while non-domestic sources remain dynamically balanced.
3. The organic nutrient ratio and transport distance positively affect instream nutrient transformation and removal, whereas upstream influx has a relatively minor impact.
4. The overall N:P ratio is close to the Redfield ratio, resulting from a high N:P ratio in NPS and a low ratio in PS, signals that dual controls on nitrogen and phosphorus reductions are necessary. The high N:P ratio in NPS is caused by an abundance of nitrogen fertilizer and soil nitrate pools, as well as a higher export ratio for nitrogen compared to phosphorus. Nitrogen variations are driven primarily by NPS, whereas phosphorus fluxes are dominated by PS. As a result, nitrogen shows greater interannual variability, while phosphorus exhibits higher overall variability.

CRediT authorship contribution statement

Ying Zhang: Writing – original draft, Visualization, Methodology, Investigation, Formal analysis. **Jianping Gan:** Writing – review & editing, Supervision, Funding acquisition, Data curation, Conceptualization.

Declaration of competing interest

The authors declare that they have no known competing financial interests or personal relationships that could have appeared to influence the work reported in this paper.

Acknowledgements

This work was supported by the Areas of Excellence Scheme (AoE/P-601/23-N, EARTH-HK project) and the General Research Fund (GRF 16307423) of the Hong Kong Research Grants Council. The Center for Ocean Research in Hong Kong and Macau is a joint ocean research center between the Laoshan Laboratory and the Hong Kong University of Science and Technology (HKUST).

Appendix A. Supplementary data

Supplementary data to this article can be found online at https://doi.org/10.1016/j.jhydrol.2025.134406.

Data availability

All data sources used in this study are publicly accessible. The detailed data for setting up and validating the model, along with their corresponding online sources, are provided in Tables 1 to 3. Processed data and scripts necessary to reproduce the analyses and figures can be found at https://ocean.hkust.edu.hk/data/paper/Zhang_JH_2025_zip.

References

Bao, W., Yang, Y., Fu, T., Xie, G.H., 2019. Estimation of livestock excrement and its biogas production potential in China. J. Clean. Prod. 229, 1158–1166. https://doi.org/10.1016/j.jclepro.2019.05.059.

Basinski, J.J., Bone, S.E., Klein, A.R., Thongsomboon, W., Mitchell, V., Shukle, J.T., Druschel, G.K., Thompson, A., Aristilde, L., 2024. Unraveling iron oxides as abiotic catalysts of organic phosphorus recycling in soil and sediment matrices. Nat. Commun. 15, 5930. https://doi.org/10.1038/s41467-024-47931-z.

Battin, T.J., Lauerwald, R., Bernhardt, E.S., Bertuzzo, E., Gener, L.G., Hall, R.O., Hotchkiss, E.R., Maavara, T., Pavelsky, T.M., Ran, L., Raymond, P., Rosentreter, J.A., Regnier, P., 2023. River ecosystem metabolism and carbon biogeochemistry in a changing world. Nature 613, 449–459. https://doi.org/10.1038/s41586-022-05500-8.

Bieger, K., Arnold, J.G., Rathjens, H., White, M.J., Bosch, D.D., Allen, P.M., 2019. Representing the connectivity of upland areas to floodplains and streams in SWAT+. JAWRA J. Am. Water Resour. Assoc. 55, 578–590. https://doi.org/10.1111/1752-1688.12728.

Bojanowski, D., Orlińska-Woźniak, P., Wilk, P., Jakusik, E., Szalińska, E., 2024. Spatial and temporal changes in nutrient source contribution in a lowland catchment within the Baltic Sea region under climate change scenarios. Water Resour. Res. 60, e2023WR034979. https://doi.org/10.1029/2023WR034979.

Brown, L.C., Barnwell, T.O., 1987. The enhanced stream water quality models QUAL2E and QUAL2E-UNCAS: Documentation and user manual. EPA Athens, GA, USA.

Chen, L., Zeng, Q., Zhang, Q., Zhu, B., Fan, Y., Yuan, X., Chen, Y., 2025. Microbial phosphorus demand affects carbon-degrading potential under long-term nitrogen addition in a subtropical forest. Appl. Soil Ecol. 211, 106154. https://doi.org/10.1016/j.apsoil.2025.106154.

Chen, S., Chen, L., Liu, X., Pan, Y., Zhou, F., Guo, J., Huang, T., Chen, F., Shen, Z., 2022. Unexpected nitrogen flow and water quality change due to varying atmospheric deposition. J. Hydrol. 609, 127679. https://doi.org/10.1016/j.jhydrol.2022.127679.

Chen, Y., Zhang, Z., Du, S., Shi, P., Tao, F., Doyle, M., 2011. Water quality changes in the world's first special economic zone, Shenzhen. China. Water Resour. Res. 47, W11515. https://doi.org/10.1029/2011WR010491.

Cheshmehzangi, A., Tang, T., 2022. China's city cluster development: from megacities development trend to urban agglomeration plan. In: China's City Cluster Development in the Race to Carbon Neutrality. Springer Nature, Singapore, pp. 25–34.

Cheung, P.T.Y., Leung, E.Y.M., 2018. The changing industrial transformation in the Pearl River Delta: issues, challenges, and intergovernmental coordination, in: Urbanization and Urban Governance in China: Issues, Challenges, and Development. Palgrave Macmillan US, New York, pp. 13–47.

Climate Data Store, 2025. Agrometeorological indicators from 1979 to present derived from reanalysis [WWW Document]. URL https://cds.climate.copernicus.eu/datasets/sis-agrometeorological-indicators?tab=overview.

Cole, L.J., Stockan, J., Helliwell, R., 2020. Managing riparian buffer strips to optimise ecosystem services: a review. Agric. Ecosyst. Environ. 296, 106891. https://doi.org/10.1016/j.agee.2020.106891.

Deng, J., Zhou, Y., Chu, L., Wei, Y., Li, Z., Wang, T., Dai, C., 2023. Spatiotemporal variations and determinants of stream nitrogen and phosphorus concentrations from a watershed in the three Gorges Reservoir Area, China. Int. Soil Water Conserv. Res. 11, 507–517. https://doi.org/10.1016/j.iswcr.2022.09.004.

Department of Ecology and Environment of Guangdong Province, 2024. URL https://gdee.gd.gov.cn/hjjce/shj.

Guangdong Statistical Bureau, 2020. Guangdong Statistical Yearbook. China Statistical Press, Beijing.

Hale, R.L., Grimm, N.B., Vörösmarty, C.J., Fekete, B., 2015. Nitrogen and phosphorus fluxes from watersheds of the northeast U.S. from 1930 to 2000: Role of anthropogenic nutrient inputs, infrastructure, and runoff. Glob. Biogeochem. Cycles 29, 341–356. https://doi.org/10.1002/2014GB004909.

Hamlin, Q.F., Kendall, A.D., Martin, S.L., Whitenack, H.D., Roush, J.A., Hannah, B.A., Hyndman, D.W., 2020. Quantifying landscape nutrient inputs with spatially explicit nutrient source estimate maps. J. Geophys. Res. Biogeosciences 125, e2019JG005134. https://doi.org/10.1029/2019JG005134.

Han, Y., Liu, Z., Chen, Y., Li, Y., Liu, H., Song, L., Chen, Y., 2023. Assessing non-point source pollution in an apple-dominant basin and associated best fertilizer management based on SWAT modeling. Int. Soil Water Conserv. Res. 11, 353–364. https://doi.org/10.1016/j.iswcr.2022.10.002.

Hildebrandt, S., Krueger, E.H., Ruhl, A.S., Borchardt, D., 2024. Efficacy of point source legislation quantified for a 64-year river water quality trajectory of phosphorus loading. J. Environ. Manage. 352, 119956. https://doi.org/10.1016/j.jenvman.2023.119956.

Hoffmann, C.C., Zak, D., Kronvang, B., Kjaergaard, C., Carstensen, M.V., Audet, J., 2020. An overview of nutrient transport mitigation measures for improvement of water quality in Denmark. Ecol. Eng. 155, 105863. https://doi.org/10.1016/j.ecoleng.2020.105863.

Huang, G., Liu, L., Liu, C., Wang, W., Han, D., 2021. Chapter 18 - Groundwater pollution of Pearl River Delta, in: Mukherjee, A., Scanlon, B.R., Aureli, A., Langan, S., Guo, H., McKenzie, A.A. (Eds.), Global Groundwater. Elsevier, pp. 251–260. https://doi.org/10.1016/B978-0-12-818172-0.00018-9.

Ismail, R., Rawashdeh, A., Al-Mattarneh, H., Hatamleh, R., Telfah, D.B., Jaradat, A., 2024. Artificial intelligence for application in water engineering: the use of ANN to determine water quality index in rivers. Civ. Eng. J. 10, 2261–2274. https://doi.org/10.28991/CEJ-2024-010-07-012.

Jain, S., Bawa, A., Mendoza, K., Srinivasan, R., Parmar, R., Smith, D., Wolfe, K., Johnston, J.M., 2025. Enhancing prediction and inference of daily in-stream nutrient and sediment concentrations using an extreme gradient boosting based water quality estimation tool - XGBest. Sci. Total Environ. 963, 178517. https://doi.org/10.1016/j.scitotenv.2025.178517.

Ju, X., Gu, B., Wu, Y., Galloway, J.N., 2016. Reducing China's fertilizer use by increasing farm size. Glob. Environ. Change 41, 26–32. https://doi.org/10.1016/j.gloenvcha.2016.08.005.

Kieu, L.D., Quoc, P.N., 2024. Spatial and temporal analysis of surface water pollution indices using statistical methods. Civ. Eng. J. 10, 1828–1841. https://doi.org/10.28991/CEJ-2024-010-06-07.

Li, J., Liang, E., Deng, C., Li, B., Cai, H., Ma, R., Xu, Q., Liu, J., Wang, T., 2024. Labile dissolved organic matter (DOM) and nitrogen inputs modified greenhouse gas dynamics: a source-to-estuary study of the Yangtze River. Water Res. 253, 121318. https://doi.org/10.1016/j.watres.2024.121318.

Li, M., Huang, L., Meng, M., Ding, X., Chen, M., Cao, Y., 2025. Species mixing increases biomass and alters architecture of fine roots, but does not affect their morphological traits: a meta-analysis of forest plantations in China. J. Environ. Manage. 392, 126899. https://doi.org/10.1016/j.jenvman.2025.126899.

Li, R., Liang, Z., Hou, L., Zhang, D., Wu, Q., Chen, J., Gao, L., 2023. Revealing the impacts of human activity on the aquatic environment of the Pearl River Estuary, South China, based on sedimentary nutrient records. J. Clean. Prod. 385, 135749. https://doi.org/10.1016/j.jclepro.2022.135749.

Liu, L., Wu, T., Xu, Z., Pan, X., 2018. The water-economy nexus and sustainable transition of the Pearl River Delta, China (1999–2015). Sustainability 10, 2595. https://doi.org/10.3390/su10082595.

Lu, S., Liu, M., Yi, J., Li, S., Xu, Y., Zhang, H., Ding, F., 2024. Lateral partition patterns and controlling factors of soil infiltration at a steep, near-stream, and humid hillslope scale. CATENA 239, 107917. https://doi.org/10.1016/j.catena.2024.107917.

Luna Juncal, M.J., Masino, P., Bertone, E., Stewart, R.A., 2023. Towards nutrient neutrality: a review of agricultural runoff mitigation strategies and the development of a decision-making framework. Sci. Total Environ. 874, 162408. https://doi.org/10.1016/j.scitotenv.2023.162408.

McDowell, R.W., Luo, D., Pletnyakov, P., Upsdell, M., Dodds, W.K., 2025. Anthropogenic nutrient inputs cause excessive algal growth for nearly half the world's population. Nat. Commun. 16, 1830. https://doi.org/10.1038/s41467-025-57054-8.

Meert, W., Hendrickx, K., Van Craenendonck, T., Robberechts, P., Blockeel, H., Davis, J., 2020. DTAIDistance. https://doi.org/10.5281/zenodo.7158824.

Mihiranga, H.K.M., Jiang, Y., Sathsarani, M.G.S., Li, X., Ritigala, T., Demissie, H., Wang, W., 2022. Identification of rainy season nitrogen export controls in a semi-arid mountainous watershed. North China. Sci. Total Environ. 839, 156293. https://doi.org/10.1016/j.scitotenv.2022.156293.

Ministry of Ecology and Environment, 2021. Manual of National Emission Source Census Pollutant Discharge Accounting Method and Coefficient [WWW Document]. URL http://www.mee.gov.cn.

Mu, X., Qiu, J., Cao, B., Cai, S., Niu, K., Yang, X., 2022. Mapping soil erosion dynamics (1990–2020) in the Pearl River Basin. Remote Sens. 14, 5949. https://doi.org/10.3390/rs14235949.

Naden, P., Bell, V., Carnell, E., Tomlinson, S., Dragosits, U., Chaplow, J., May, L., Tipping, E., 2016. Nutrient fluxes from domestic wastewater: a national-scale

historical perspective for the UK 1800–2010. Sci. Total Environ. 572, 1471–1484. https://doi.org/10.1016/j.scitotenv.2016.02.037.
Nakayama, Y., Arreguin, S., Leon, P., Douglass, M., Becker, T., Margenot, A.J., 2025. Nitrogen losses under soybean production are mitigated by substituting ammonium phosphates with triple superphosphate but non-fertilizer losses remain appreciable. Agric. Ecosyst. Environ. 378, 109274. https://doi.org/10.1016/j.agee.2024.109274.
National Bureau of Statistics, 2021a. National Census [WWW Document]. URL https://www.stats.gov.cn/sj/pcsj/.
National Bureau of Statistics, 2021b. China Urban and Rural Construction Statistical Yearbook, 1990–2020. China Statistical Press, Beijing.
National Bureau of Statistics, 2021c. China Hydrological Yearbook, 2018–2023. China Statistical Press, Beijing.
National Cryosphere Desert Data Center, 2025. URL http://www.ncdc.ac.cn.
National Environmental Monitoring Centre, 2019. Weekly Report on Automatic Water Quality Monitoring, 2004–2018.
Nespoulous, J., Merino-Martín, L., Monnier, Y., Bouchet, D.C., Ramel, M., Dombey, R., Viennois, G., Mao, Z., Zhang, J.-L., Cao, K.-F., Le Bissonnais, Y., Sidle, R.C., Stokes, A., 2019. Tropical forest structure and understorey determine subsurface flow through biopores formed by plant roots. CATENA 181, 104061. https://doi.org/10.1016/j.catena.2019.05.007.
Ongley, E.D., Xiaolan, Z., Tao, Y., 2010. Current status of agricultural and rural non-point source pollution assessment in China. Env. Pollut 158, 1159–1168. https://doi.org/10.1016/j.envpol.2009.10.047.
Ptacnik, R., Andersen, T., Tamminen, T., 2010. Performance of the redfield ratio and a family of nutrient limitation indicators as thresholds for phytoplankton N vs. P. LimitationEcosystems 13, 1201–1214. https://doi.org/10.1007/s10021-010-9380-z.
Richards, G., Gilmore, T.E., Mittelstet, A.R., Messer, T.L., Snow, D.D., 2021. Baseflow nitrate dynamics within nested watersheds of an agricultural stream in Nebraska, USA. Agric. Ecosyst. Environ. 308, 107223. https://doi.org/10.1016/j.agee.2020.107223.
Rideout, J.R., Caporaso, G., Bolyen, E., McDonald, D., Baeza, Y.V., Alastuey, J.C., Pitman, A., Morton, J., Navas, J., Gorlick, K., Debelius, J., Xu, Z., llcooljohn, adamrp, Shorenstein, J., Luce, L., Treuren, W.V., charudatta-navare, Gonzalez, A., Brislawn, C.J., Patena, W., Schwarzberg, K., teravest, Reeder, J., shiffer1, Sfiligoi, I., nbresnick, Zhu, Q., Murray, D.K.D., Sharma, K., 2023. biocore/scikit-bio: scikit-bio 0.5.9: Maintenance release. https://doi.org/10.5281/zenodo.8209901.
Santis, A., Arbeláez, O., Cardenas, L.A., Castellanos, J., Velasquez, P., 2024. Optimizing Cr(VI) reduction in plastic chromium plating wastewater: particle size, irradiation, titanium dose. Emerg. Sci. J. 8, 17–27. https://doi.org/10.28991/ESJ-2024-08-01-02.
Statistics Bureau of Guangdong Province, 2022. Guangdong Statistical Yearbook, 1990–2020. China Statistical Press, Beijing.
Statistics Bureau of Guangdong Province, 2021. Guangdong Agricultural Yearbook, 1990–2020. China Statistical Press, Beijing.
Sun, D., Wang, X., Yu, M., Ouyang, Z., Liu, G., 2023. Dynamic evolution and decoupling analysis of agricultural nonpoint source pollution in Taihu Lake Basin during the urbanization process. Environ. Impact Assess. Rev. 100, 107048. https://doi.org/10.1016/j.eiar.2023.107048.
Tang, W., Pei, Y., Zheng, H., Zhao, Y., Shu, L., Zhang, H., 2022. Twenty years of China's water pollution control: experiences and challenges. Chemosphere 295, 133875. https://doi.org/10.1016/j.chemosphere.2022.133875.
The State Council of the People's Republic of China, 2019. Outline development plan for the Guangdong-Hong Kong-Macao Greater Bay Area.
Walton, C.R., Zak, D., Audet, J., Petersen, R.J., Lange, J., Oehmke, C., Wichtmann, W., Kreyling, J., Grygoruk, M., Jabłońska, E., Kotowski, W., Wiśniewska, M.M., Ziegler, R., Hoffmann, C.C., 2020. Wetland buffer zones for nitrogen and phosphorus retention: Impacts of soil type, hydrology and vegetation. Sci. Total Environ. 727, 138709. https://doi.org/10.1016/j.scitotenv.2020.138709.
Wang, P., Han, D., Zhang, C., Yu, F., Wang, X., Huang, P., Zhang, G., Liu, S., 2024. Integrative analysis of nutrient dynamics and its hydrological pathways in a tropical montane forest watershed: implications for landscape management. CATENA 246, 108419. https://doi.org/10.1016/j.catena.2024.108419.
Water Resources Department of Guangdong Province, 2021. Guangdong Provincial Water Resources Bulletin, 1990–2020. Guangdong.
World Bank, 2015. The world bank annual report.
Yang, Y., Yuan, Y., Xiong, G., Yin, Z., Guo, Y., Song, J., Zhu, X., Wu, J., Wang, J., Wu, J., 2024. Patterns of nitrate load variability under surface water-groundwater interactions in agriculturally intensive valley watersheds. Water Res. 267, 122474. https://doi.org/10.1016/j.watres.2024.122474.
Yao, Z., Wang, Y., Li, A., 2009. Primary analysis of water distribution ratio variation in main waterway in Pearl River Delta (in chinese). Pearl River 2 (43–45), 51.
Yu, X., Pan, Y., Song, W., Li, S., Li, D., Zhu, M., Zhou, H., Zhang, Y., Li, D., Yu, J., Wang, X., Wang, X., 2020. Wet and dry nitrogen depositions in the Pearl River Delta, South China: observations at three typical sites with an emphasis on water-soluble organic nitrogen. J. Geophys. Res. Atmospheres 125, e2019JD030983. https://doi.org/10.1029/2019JD030983.
Zeng, W., Xiang, W., Zhou, B., Ouyang, S., Zeng, Y., Chen, L., Zhao, L., Valverde-Barrantes, O.J., 2020. Effects of tree species richness on fine root production varied with stand density and soil nutrients in subtropical forests. Sci. Total Environ. 733, 139344. https://doi.org/10.1016/j.scitotenv.2020.139344.
Zhang, X., Liu, L., Chen, X., Gao, Y., Xie, S., Mi, J., 2021. GLC_FCS30: global land-cover product with fine classification system at 30 m using time-series Landsat imagery. Earth Syst. Sci. Data 13, 2753–2776. https://doi.org/10.5194/essd-13-2753-2021.
Zhang, Y., Gan, J., Yang, Q., 2024. Spatiotemporal variability of streamflow in the Pearl River Basin: controls of land surface processes and atmospheric impacts. Hydrol. Process. 38, e15151. https://doi.org/10.1002/hyp.15151.